JOURNAL OF SPACECRAFT AND ROCKETS
Vol. 38, No. 1, January–February 2001

Active Acoustic Control of a Rocket Fairing Using Spatially Weighted Transducer Arrays

Steven A. Lane*
Jackson and Tull Engineering, Albuquerque, New Mexico 87106
Jonathan D. Kemp†
Duke University, Durham, North Carolina 27708
Steven Griffin‡
U.S. Air Force Research Laboratory, Kirtland Air Force Base, New Mexico 87117
and
Robert L. Clark§
Duke University, Durham, North Carolina 27708

A preliminary study, including experimental results for a novel active acoustic control approach to reduce the low-frequency modal response in a rocket fairing, is presented. The control method uses spatially weighted transducer arrays with H_2 feedback control laws to attenuate globally the targeted acoustic modes. The nature of the fairing acoustic problem is described, the theory of the control approach is discussed, and important feasibility issues regarding the actual implementation of the control method are presented. Several controllers were implemented on a full-scale composite model of a small rocket fairing. The results demonstrate that the controller was able to reduce the response of the low-frequency modes by 6–12 dB with very little spillover. In addition, a spatially averaged reduction of the acoustic response of the fairing interior in excess of 3 dB over the 20–200-Hz bandwidth was demonstrated. The feasibility studies indicate that limitations on actuator power and volumetric displacement under actual launch conditions are not necessarily prohibitive, but may be satisfied with continued development of actuator technology and placement optimization.

Nomenclature

$\boldsymbol{A}_c, \boldsymbol{B}_c, \boldsymbol{C}_c, \boldsymbol{D}_c$	=	state-space representation of a dynamic control law
$\boldsymbol{A}'_c, \boldsymbol{B}'_c, \boldsymbol{C}'_c, \boldsymbol{D}'_c$	=	state-space representation of the control law augmented with spatial weighting vectors or matrices
$\boldsymbol{G}_{\text{act}}(j\omega)$	=	frequency response of the actuator transfer function relating the applied control signal to the actuator output signals
$\boldsymbol{G}_{\text{mic}}(j\omega)$	=	frequency response of the microphone transfer function relating the measured pressure to the output signal, V/Pa
$\boldsymbol{G}(s)$	=	Laplace transform of the system transfer matrix
$\boldsymbol{H}(j\omega)$	=	frequency response of the control law, V/V
I_{rms}	=	root mean square of the current acting on an actuator at a frequency, A
$i_s(j\omega)$	=	current signal applied to the actuators, A
P_{av}	=	average power delivered to an actuator at a frequency, W
$p(j\omega)$	=	microphone pressure measurement, Pa
$\hat{p}(j\omega)$	=	scaled pressure signal, Pa
p_{ref}	=	reference pressure, 20 μPa
R	=	resistance of the series resistor contained in the constant volume-velocity actuators, Ω
$\boldsymbol{u}$	=	vector of control inputs
u_m	=	denotes the mth system input
$\hat{u}(s)$	=	spatially weighted system input
V_{rms}	=	root-mean-square voltage acting on an actuator at a frequency, V
$v_a(j\omega)$	=	control signal applied to an actuator, V
$v_r(j\omega)$	=	voltage measured across the series resistor of an actuator circuit, V
$v_s(j\omega)$	=	voltage applied to a speaker in the control experiments, V
$\boldsymbol{W}_u$	=	spatial weighting matrix for actuators
$\boldsymbol{W}_y$	=	spatial weighting matrix for sensors
$\boldsymbol{w}_u$	=	spatial weighting vector applied to actuators
$\boldsymbol{w}_y$	=	spatial weighting vector applied to sensors
$x(j\omega), \dot{x}(j\omega)$	=	diaphragm displacement, m, and velocity, m/s, respectively
$\boldsymbol{y}$	=	vector of system outputs
$\hat{y}(s)$	=	spatially weighted system output
α	=	constant scaling factor for microphone signals
θ	=	power factor of an actuator (speaker)
$\omega_{\max}$	=	maximum frequency of measured data, rad/s
$\omega_{\min}$	=	minimum frequency of measured data, rad/s

Superscript

T	=	transpose operator

Introduction

THE high-level, low-frequency acoustic excitation that occurs at launch can induce structural-acoustic vibrations that cause payload damage. As engineers endeavor to create larger, lightweight fairings, that is, launch vehicles, acoustic excitation becomes a more critical factor in payload launch survivability. Research in acoustic attenuation within the fairing has investigated the use of both active control and passive treatments, in addition to controlling the vibration of the fairing itself.[1–5] At low frequencies, lightly damped modes dominate the interior acoustic response of the fairing. The ineffectiveness of passive treatments, such as acoustic blankets, fiberglass, and acoustic foam, at low frequencies impels consideration of active control methods.

Received 11 May 2000; revision received 15 September 2000; accepted for publication 30 September 2000.

*Research Scientist, Space and Aeronautics Technology Division, 1900 Randolph Road, SE, Ste. H. Member AIAA.
†Graduate Research Assistant, Department of Mechanical Engineering and Material Science, Box 90302. Member AIAA.
‡Basic Research Manager, Spacecraft Component Technologies Branch, 3550 Aberdeen Avenue, Kirtland. Member AIAA.
§Professor, Department of Mechanical Engineering and Material Science, Box 90300. Member AIAA.

Previous work has shown that dissipative control can be achieved in one-dimensional acoustic enclosures by using a collocated pressure sensor and a constant volume-velocity source.[6,7] This approach was extended to control low-frequency modes in an aircraft fuselage by utilizing arrays of spatially weighted sensors and actuators. The transducer arrays were spatially weighted to selectively couple with low-frequency modes, which has the advantage of reducing the order of the control law. Significant damping of the low-frequency modes was achieved without producing significant spillover.[8] Here, this control approach is extended to the fairing problem.

The present work proposes to attenuate the response of low-frequency acoustic modes in a launch vehicle fairing by using an active feedback controller in conjunction with an array of nearly collocated microphones and moving-coil actuators (speakers). Collocation reduces the phase lag between the sensors and actuators and, packaged as a single unit, limits the spatial impact of the system on the payload volume of the fairing. Spatially weighting the array of sensors (microphones) allows measurements taken by each individual sensor to be used collectively, forming a more accurate measurement of the acoustic dynamics of the enclosure. The weighting process emphasizes the coupling with the target mode or modes to be controlled and reduces the coupling with nontarget modes. Likewise, collective implementation of the actuator array enables greater control authority over the low-frequency acoustic modes. Spatial weighting results in a simplified system identification process and control law design. Because only low-frequency modes are targeted by the controller, control can be achieved with relatively low-order control laws, that is, less than 20 states. By the incorporation of low-order dynamic control laws with nearly collocated pressure sensors and volume-velocity actuators, significant controller rolloff is achieved both above and below the control bandwidth, which increases the performance and stability of the controller.

This report presents the results of a preliminary investigation of this control approach applied to a full-scale composite model of a small fairing at Duke University. Primarily, this investigation sought to determine the effectiveness of the control approach in reducing the response of the low-frequency acoustic modes of the fairing. Additionally, this work investigated the feasibility of using the control approach in an actual launch vehicle, where the overall acoustic levels exceed 140 dB over the bandwidth of 10 Hz–10 kHz.

The following discourse first focuses on the fairing acoustics, the spatial-weighting concept and its application, and the method for designing and implementing control laws. Then a discussion is presented that addresses the primary concerns regarding feasibility and the methods used here to investigate these concerns. Next, the experimental testbed, hardware, facilities, and procedure are described. Results from several controllers are presented to provide an indication of controller performance and to illustrate important controller design issues. Finally, conclusions based on this preliminary effort are given.

Theory

Fairing Acoustics

A rocket fairing is essentially a flexible, thin-walled structure that protects the payload during launch. Fairings are typically constructed of metal, such as aluminum, but more recently composites have been used. Although composites offer many advantages, they are less massive and, therefore, allow increased transmission of exterior disturbances. Acoustic waves within the fairing interact detrimentally with the payload. Typically, the overall acoustic levels inside small fairings during launch can exceed 140 dB. At low frequencies (10–200 Hz), the levels reach approximately 120–130 dB.

The length of the fairing considered in this work was 5.3 m, and the maximum diameter was approximately 1.3 m. For this geometry, the low-frequency acoustic modes are longitudinal. A model of a rigid-walled cylinder of similar dimensions provides a reasonable prediction of the lowest acoustic natural frequencies of the fairing. If the longitudinal mode-shapes can be approximated as cosine functions, the first three acoustic natural frequencies occur at approximately 32, 65, and 97 Hz, with the corresponding wavelengths being 10.6, 5.3, and 3.5 m (Ref. 9). Though a very rough approximation, it is apparent that at such long wavelengths passive damping treatments such as acoustic blankets and liners are impractical.

Because of the low amount of damping provided by the fairing, the low-frequency acoustic modes are lightly damped, further exacerbating the problem. If the payload exhibited a structural resonance near an acoustic resonance, the acoustic loading could cause damage to the payload. Flat surfaces of solar panels and lightweight structures such as thin films and membranes would be especially susceptible to damage from low-frequency excitation.

The acoustic modes of the fairing are excited by a number of disturbance sources, including aerodynamic buffeting during flight, structural vibrations induced by the rocket motors, and pyrotechnic shocks during stage separations. These sources act in addition to the explosive noise produced by the motors themselves. The presence of multiple, random disturbance sources precluded adaptive feedforward control and compelled the use of active feedback control in the present investigation.

Spatial Weighting

Previous research has demonstrated the advantages of employing spatially weighted, discrete transducer arrays to emphasize coupling with target modes.[8,10–14] Applications have typically involved structural systems where the sensors and actuators were spatially weighted to couple with particular modes of the structure. Sensor and actuator weights were related to the mode shape of the structure and the relative positions of the sensors and actuators. To illustrate spatial weighting for a one-dimensional acoustic application, consider the rigid-walled, simply supported cylinder presented in Fig. 1a, with sensors mounted along the length as indicated. The corresponding first acoustic mode for this hypothetical system is presented in Fig. 1b. The appropriate spatial weight for each of the actuators shown corresponds to the modal amplitude evaluated at the sensor position. Notice that the spatial-weighting values for the first three sensors are positive, whereas the last three are negative. The change of sign indicates that the last three sensors are 180 deg out of phase with the first three. The fourth sensor is located near the node of the mode shape; therefore, its corresponding spatial weight would be near zero.

For complex structures and enclosures such as the fairing, the spatial-weighting vector or matrix must be determined from experimental measurements. The method presented herein estimates the appropriate spatial-weighting vector from frequency-response measurements. Because the sensors and actuators in the experiments were collocated with respect to the acoustic wavelength, the spatial weight for each actuator was approximated as the weight determined for the corresponding sensor. This approximation is sufficient for control of low-frequency modes in a lightly damped enclosure.

Consider an enclosure with an array of pressure sensors (microphones) positioned arbitrarily throughout. A loudspeaker is positioned arbitrarily in the enclosure to provide a stochastic noise input. The frequency responses between the noise input and the sensor microphones reveal the degree of coupling between each sensor and the acoustic modes of the enclosure.[8] At a particular modal frequency, the weight for a given sensor can be defined as the real part of the complex frequency response of the sensor at the modal frequency. Weights are calculated for each sensor in this fashion from the respective frequency-response measurements. The weights collectively form a vector of weighting values for the sensor array and,

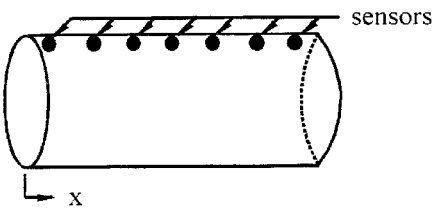

Fig. 1a Simply supported cylinder.

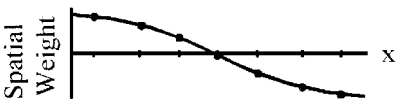

Fig. 1b Fundamental acoustic mode shape.

hence, for the actuator array. The weighting vector is normalized to unity for convenience.

Consider a system with M inputs $\boldsymbol{u}$ and P outputs $\boldsymbol{y}$, represented by the transfer matrix $\boldsymbol{G}(s)$. The spatial-weighting vector used to emphasize a single target mode is denoted as $\boldsymbol{w}_y$ for the sensors and $\boldsymbol{w}_u$ for the actuators, where

$$\boldsymbol{w}_y = \boldsymbol{w}_u^T \tag{1}$$

Application of the weighting vectors $\boldsymbol{w}_u$ and $\boldsymbol{w}_y$ to the system inputs and outputs, respectively, reduces the system to a single input $\hat{u}(s)$ and a single output $\hat{y}(s)$. The output is expressed as a linear combination of the sensor measurements,

$$\hat{y}(s) = \boldsymbol{w}_y \boldsymbol{y} \tag{2}$$

Because the sensor outputs can be expressed as

$$\boldsymbol{y} = \boldsymbol{G}(s)\boldsymbol{u} \tag{3}$$

substituting Eq. (3) into Eq. (2) yields

$$\hat{y}(s) = \boldsymbol{w}_y \boldsymbol{G}(s)\boldsymbol{u} \tag{4}$$

Because the inputs to the plant are given as

$$u_m = \boldsymbol{w}_{u_m} \hat{u}, \qquad m = 1, 2, \ldots, M \tag{5}$$

the output can be expressed as

$$\hat{y}(s) = \sum_{p=1}^{P} \boldsymbol{w}_{y_p} \sum_{m=1}^{M} \boldsymbol{G}_{p,m}(s) \boldsymbol{w}_{u_m} \hat{u}(s) \tag{6}$$

which yields

$$\frac{\hat{y}(s)}{\hat{u}(s)} = \sum_{p=1}^{P} \sum_{m=1}^{M} \boldsymbol{w}_{y_p} \boldsymbol{G}_{p,m}(s) \boldsymbol{w}_{u_m} \tag{7}$$

Therefore, the resulting single-input/single-output system is expressed as

$$\hat{y}(s)/\hat{u}(s) = \boldsymbol{w}_y \boldsymbol{G}(s) \boldsymbol{w}_u \tag{8}$$

For a system where Q modes are to be selected for control, the order (i.e., the number of inputs and outputs, as opposed to the number of states) of the system is expanded from a single-input/single-output system to one having an input and output corresponding to each targeted mode. In this case, the weighting vectors are replaced by the matrices $\boldsymbol{W}_u$ and $\boldsymbol{W}_y$ ($M \times Q$ and $Q \times P$, respectively) with rows and columns corresponding to the spatial-weighting vector for each target mode.

To achieve global dissipation of acoustic energy in the fairing, a measurement or linear combination of states differing from that of the sensors must be included, otherwise control effects may only be local, that is, limited to servocontrol. In this investigation, this measurement, referred to as the performance signal, was generated by using a second array of microphones distributed arbitrarily throughout the interior of the fairing. Measurements from these performance microphones were not measured by the controller, but were only used as a performance metric in the design of the control law. Spatial-weighting vectors were measured and applied to the performance microphones to emphasize the same modes targeted by the controller.

Control Design

Dynamic controllers can be shaped to emphasize control over a specific bandwidth and to produce rolloff above the control bandwidth. Therefore, dynamic controllers can provide better performance and increased stability in comparison to static gain controllers. The control laws used in the present work were computed to minimize the two norm H_2 of the transfer matrix between the performance variables and the exogenous inputs.[12,15] Criteria for control law design included disturbance rejection at low frequencies while maintaining low sensitivity to noise and modeling errors at higher frequencies.

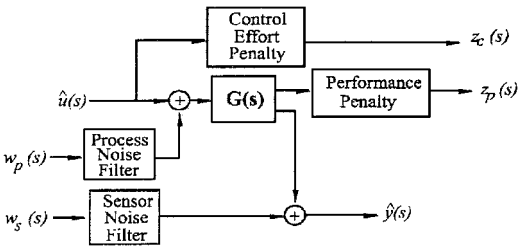

Fig. 2 Block diagram of the augmented plant used in H_2 control law synthesis.

In the subsequent experiments, models of the open-loop system were computed by using an approach based on the eigensystem realization algorithm.[16] This method of system identification yielded low-order, discrete state-space models that were used in control law synthesis. Frequency-dependent weighting filters were added to the open-loop system model to form the augmented plant presented in Fig. 2. The inputs to the augmented plant included the control signal $\hat{u}(s)$, the process noise input that represents exogenous inputs and disturbances $w_p(s)$, and the sensor noise input $w_s(s)$. The outputs of the augmented plant included the control effort penalty $z_c(s)$, the spatially weighted performance microphone measurements $z_p(s)$, and the sensed variable $\hat{y}(s)$, which represents the spatially weighted sensor microphone measurements.

For system modeling, the disturbance loudspeaker and the acoustic paths from the disturbance to the performance microphones were not measured or included. This exclusion prevented the controller from attempting to impedance load the disturbance. Instead, the controller should yield attenuation regardless of the source or the location of the disturbance. For modeling purposes, the process noise input was summed into the control input (see Fig. 2). Therefore, the plant (fairing acoustics) shaped the effects of the process noise as recommended.[12] To generate a well-posed control problem, a low-pass filter was added to the process noise input to eliminate feedthrough terms. The cutoff frequency of the low-pass filter was set to 10 kHz, well above the bandwidth of interest.

The augmented system was assembled and modeled using Simulink,[17] and H_2 control laws were computed using MATLAB®.[18] Filters used to shape the controller increased the order (number of states) of the augmented plant and of the resulting control law. This resulted in a control law of much larger order than necessary. Model reduction techniques, such as balanced residualization or truncation,[15,19] were applied to reduce the order of the controller without significantly affecting the dynamics of the controller or the closed-loop system.

After computation, the reduced-order control law was transformed into the discrete domain using a Tustin transformation, the spatial-weighting vectors were applied, and the control law was downloaded to a digital signal processor (DSP) for implementation. A control law given as $\{\boldsymbol{A}_c, \boldsymbol{B}_c, \boldsymbol{C}_c, \boldsymbol{D}_c\}$ can be expanded for $M = P$ collocated sensors and actuators such that

$$\boldsymbol{A}_c' = \boldsymbol{A}_c, \qquad \boldsymbol{C}_c' = \boldsymbol{w}_u \boldsymbol{C}_c, \qquad \boldsymbol{B}_c' = \boldsymbol{B}_c \boldsymbol{w}_y, \qquad \boldsymbol{D}_c' = \boldsymbol{w}_u \boldsymbol{D}_c \boldsymbol{w}_y \tag{9}$$

For a multimode ($Q > 1$) controller, the weighting vectors are replaced by the corresponding weighting matrices.

Controller performance was determined by comparing the open-loop and closed-loop frequency-response functions from a disturbance input (band-limited random noise) to the performance microphone array and the sensor microphone array. Averaging these frequency-response measurements provided representative open-loop and closed-loop frequency responses and facilitated evaluation of the overall effects of the controller as a function of frequency. From this evaluation, the occurrence of spillover, the degree of coupling to the target modes, and the average amount of attenuation at the sensors and globally at the performance microphones can be observed.

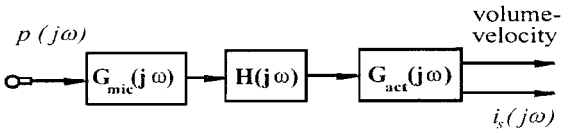

Fig. 3 Path from sensor to actuator.

Feasibility Issues

An active control system must meet many criteria to be practical in a launch vehicle. The additional weight and expense of the control system is of primary concern. Another important consideration is the performance-to-weight ratio, which indicates how much attenuation is provided for a given weight of the control system. In some situations, it might be determined that simply adding an equivalent amount of mass to the structure would provide the same attenuation levels without the additional complexity.

In this investigation, issues such as actuator power requirements, actuator diaphragm displacement, and signal clipping were considered. Although the controller would only operate for the several minutes between launch and orbit, it is important to determine the amount of power required by the controller (specifically the actuators) to determine feasibility from a power-supply/battery standpoint. Another important issue involves the response of the actuator to the control input. A control signal for high-level disturbances could command a response beyond reasonable actuator abilities, such as an extreme volumetric displacement. By the measurement of the response of the actuators and the transfer function from the sensor inputs to the actuators, the power and diaphragm displacement were extrapolated from the experimental data to higher sound pressure levels. Although the relatively low sound pressure levels used in these preliminary experiments (90 dB) deemed clipping an unimportant issue, clipping would be a critical consideration in an actual implementation where the acoustic disturbance is orders of magnitude larger.

The path from the sensor input to the actuator output is presented in Fig. 3. The pressure response measured at each sensor, $p(j\omega)$, for a band-limited random disturbance was used as a rough approximation of the pressure response that would be experienced in the fairing at launch. The microphone response was integrated over the bandwidth to compute the total rms pressure at the microphone. The total rms pressure was then converted to sound pressure level [SPL(dB)], which is given by

$$\mathrm{SPL(dB)} = 20\log_{10}\left(\frac{\sqrt{\sum_{i=\omega_{\min}}^{\omega_{\max}} |p(j\omega_i)|^2}}{p_{\mathrm{ref}}}\right) \tag{10}$$

By scaling the sound pressure level [$\hat{\mathrm{SPL}}$(dB)] spectrum measured at lower disturbance levels, the pressure spectrum corresponding to the total rms pressure for any desired level can be predicted, that is,

$$\hat{\mathrm{SPL}}\mathrm{(dB)} = 20\log_{10}\left(\frac{\sqrt{\sum_i \alpha^2 |p(j\omega_i)|^2}}{p_{\mathrm{ref}}}\right) \tag{11}$$

where α is a constant scaling factor for each microphone and is determined by

$$\alpha = \frac{p_{\mathrm{ref}} 10^{\hat{\mathrm{SPL}}/20}}{\sqrt{\sum_i |p(j\omega_i)|^2}} \tag{12}$$

where $\hat{\mathrm{SPL}}$ is the desired SPL. This scaling yields a rough prediction of the pressure measurement $\hat{p}(j\omega)$ that would occur for an actual launch,

$$\hat{p}(j\omega) = \alpha p(j\omega) \tag{13}$$

Each microphone transduced the pressure inside the fairing to an equivalent output voltage that was defined by the microphone sensitivity. This signal was then filtered and amplified by the microphone conditioning hardware. Thus, the gain of the microphone conditioning circuitry and the microphone sensitivity, collectively referred to as $\boldsymbol{G}_{\mathrm{mic}}(\boldsymbol{j\omega})$, were necessary for calculating the interior SPLs from the output signals of the microphone conditioning hardware.

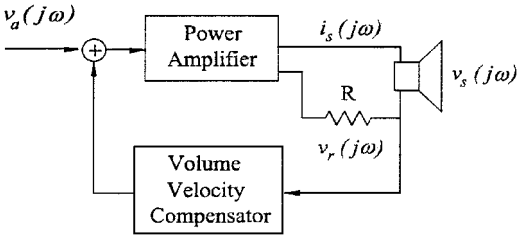

Fig. 4 Schematic of the actuator setup.

For feedback controller implementation, the voltage signals from the sensor microphones and the conditioning hardware were sampled by the DSP and filtered by the discrete control law to compute the control signals. The control law, which is referred to as $\boldsymbol{H}(\boldsymbol{j\omega})$, was characterized by measuring the frequency response across the input and output channels of the DSP. This measurement verified that the dynamics of the downloaded controller corresponded to the designed control law and revealed any effects from antialiasing and reconstruction filters of the DSP.

The output voltages from the DSP as applied to the actuators, denoted as $v_a(j\omega)$, were predicted by using the controller transfer matrix $\boldsymbol{H}(\boldsymbol{j\omega})$, the transfer functions across the microphones $\boldsymbol{G}_{\mathrm{mic}}(\boldsymbol{j\omega})$, and the estimated pressure signals acting on the microphones $\hat{p}(j\omega)$,

$$v_a(j\omega) = \boldsymbol{H}(\boldsymbol{j\omega})\boldsymbol{G}_{\mathrm{mic}}(\boldsymbol{j\omega})\hat{p}(j\omega) \tag{14}$$

From this prediction, the controller voltages were estimated as a function of fairing interior sound level for a given controller.

As shown in Fig. 4, the actuator hardware included a power amplifier, a moving-coil speaker, a series resistor for sensing the current, and a constant volume-velocity compensator. In the subsequent experiments, 14-cm-diam loudspeakers mounted in small enclosures were used as control actuators. Each loudspeaker system was compensated by using a feedback loop around the actuator to cause the loudspeaker to approximate constant volume-velocity behavior over the control bandwidth.[7] This feedback loop reduced the effects of the loudspeaker dynamics on the closed-loop system and simplified control law design.

The diaphragm velocity $\dot{x}(j\omega)$ and displacement $x(j\omega)$ were measured as a function of voltage applied to the actuator $v_a(j\omega)$ using a laser vibrometer. The frequency response of the actuator displacement to applied voltage was used to extrapolate the actuator displacement corresponding to higher SPLs. This calculation assumes linearity and ignores possible peak-to-peak voltage limits of the DSP. Although free-air measurements give a good estimate of the velocity and displacement response, they do not account for the coupling between the actuator and the acoustic system. In the coupled system, the acoustic modes of the fairing affect the actuator response. However, these effects are small and were neglected in the present study.

For a voltage applied to an actuator, the average power delivered to the speaker can be computed as[20]

$$P_{\mathrm{av}} = V_{\mathrm{rms}} I_{\mathrm{rms}} \cos\theta \tag{15}$$

The power spectrum of the voltage applied to a speaker can be calculated by using the frequency-response function $v_s(j\omega)/v_a(j\omega)$:

$$|v_s(j\omega)|^2 = \left|\frac{v_s(j\omega)}{v_a(j\omega)}\right|^2 |v_a(j\omega)|^2 \tag{16}$$

where $v_s(j\omega)$ is the voltage acting on the speaker as shown in Fig. 4. The power spectrum of the current $i_s(j\omega)$ is readily available by dividing the frequency response of the series resistor voltage signal to the applied voltage by the series resistor resistance, which yields

$$|i_s(j\omega)|^2 = \left|\frac{v_r(j\omega)}{R v_a(j\omega)}\right|^2 |v_a(j\omega)|^2 \tag{17}$$

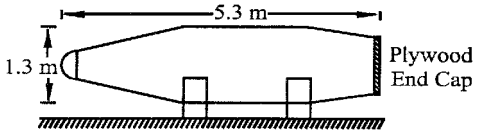

Fig. 5 Illustration of the fairing testbed.

The power delivered to a speaker as a function of frequency for an applied voltage $v_a(j\omega)$ is computed from

$$P_{\text{av}}(j\omega) = \sqrt{|v_s(j\omega)|^2}\sqrt{|i_s(j\omega)|^2}\cos\theta(j\omega) \tag{18}$$

This can be summed over the bandwidth to yield an overall actuator (OA) power requirement, computed as

$$P_{\text{OA}} = \sqrt{\sum_{i=\omega_{\min}}^{\omega_{\max}} P_{\text{av}}^2(j\omega_i)} \tag{19}$$

Experimental Equipment and Testbed

Experiments were conducted on a full-scale composite fairing model using 16 constant volume-velocity actuators with 16 collocated sensor microphones and 16 performance microphones. The fairing (shown in Fig. 5) was approximately 5.3 m in length, 1.3 m in diameter (maximum), and tapered at both ends. An aluminum end cap was fixed to the nose, and a plywood end cap was attached to the base. Each sensor/actuator pair was rigidly attached to the composite structure. The sensor/actuator pairs were evenly distributed along the length and circumference of the fairing interior to yield unbiased spatial sampling. For these experiments, off-the-shelf loudspeakers that were rated at 100 W with a maximum linear excursion of 4.5 mm were used as actuators. A disturbance loudspeaker was placed in the corner of the fairing near the base end cap and was used to excite the interior cavity modes. The performance microphones were distributed throughout the interior at arbitrary positions to measure the overall controller effects. All cabling was connected through a panel at the base of the fairing. The controller, spectrum analyzers, power amplifiers, microphone conditioners, and other required hardware were housed outside of the fairing. A block diagram of the setup is presented in Fig. 6.

Both the sensor and performance microphones were calibrated, ICP devices that, according to the manufacturer's specifications, were accurate to within ±1 dB over the bandwidth of 20–7000 Hz and were linear within 3% up to 128 dB. Stated temperature effects were less than ±0.5 dB over the range of −20–65°C. The microphone conditioning hardware provided 12-bit accuracy and 72-dB channel isolation and had a low-frequency response of ±5% at 0.5 Hz and a high-frequency response of ±5% at 100 kHz. Because the control bandwidth in these experiments was roughly 20–200 Hz, the uncertainty of the conditioning hardware was conservatively assumed to be 3%. The accuracy of the laser vibrometer used to characterize the actuators was specified by the manufacturer to be within 3% over its bandwidth.

Multichannel Rane amplifiers were used to drive the actuators. Each amplifier channel was ac coupled and was capable of approximately 100 W. Amplifier specifications included a 103-dB signal-to-noise ratio, and −60-dB cross-talk. The frequency response was measured to be flat (0 dB) from 20 Hz to over 10 kHz. A Siglab spectrum analyzer system was used to generate disturbance signals and to measure open- and closed-loop frequency responses. The analyzer used a 20-bit analog-to-digital converter and an 18-bit digital-to-analog converter. The manufacturer's specifications indicated an absolute accuracy of 0.0025% of full-range, 90-dB alias protection and greater than 90-dB dynamic range. The DSP used for implementing the control law was a 32-bit TMS320C40 processor that used 16-bit converters.

The greatest source of experimental uncertainty originated from the microphones, microphone conditioning hardware, and the vibrometer measurements. The resulting uncertainty of the microphones and the microphone conditioning hardware was assumed to be the product of the uncertainties, which yielded approximately 6.1%, that is, 1.03 × 1.03. This is equivalent to an experimental error range of approximately ±0.51 dB over the control bandwidth. For the vibrometer measurements, the experimental error range was only ±0.26 dB across the bandwidth.

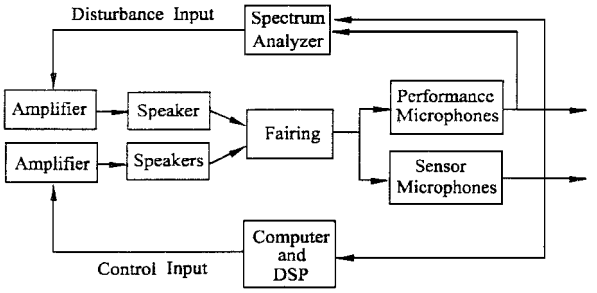

Fig. 6 Schematic of the experimental setup.

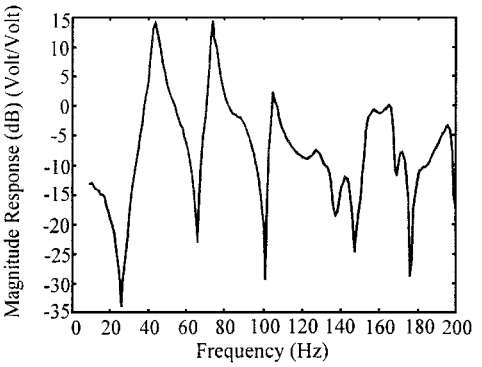

Fig. 7 Representative response at a sensor microphone (± 0.51-dB uncertainty).

Results

Sensors

The response measured at a representative sensor microphone for band-limited (200-Hz) random noise acting on the disturbance loudspeaker is shown in Fig. 7. The response clearly indicates the lightly damped modal nature of the fairing interior. From this frequency-response function, the resulting interior SPL for a unit-magnitude voltage (rms) applied to the disturbance loudspeaker can be determined. Including the microphone sensitivity of 20.61 mV/Pa and the conditioning hardware gain of 50, the voltage response in Fig. 7 can be converted to pascal per volt, where

$$\frac{\text{pressure (Pa)}}{\text{disturbance (V)}} = \left(\frac{1\text{ Pa}}{20.61\text{ mV}}\right)\left(\frac{1000\text{ mV}}{\text{V}}\right)\left(\frac{1\text{ V}}{50\text{ V}}\right) \times \left(\frac{\text{microphone voltage output}}{\text{disturbance voltage input}}\right)$$

For a band-limited random noise disturbance input of 1 V rms, the resulting rms pressure response at this microphone would be approximately 117 dB (relative to a reference pressure of 20 μPa). To scale this pressure spectrum such that the rms pressure level was 120 dB, the scaling factor α, determined from Eq. (12), would be approximately 1.275.

Actuators

The diaphragm velocity response as measured with a laser vibrometer relative to a 1-V rms band-limited random noise input $v_a(j\omega)$ for a typical actuator is presented in Fig. 8. Figure 8 shows the open-loop velocity response and the closed-loop response with the constant volume-velocity compensator. The diaphragm velocity of the compensated actuator was nearly constant at roughly 18 mm/s/V

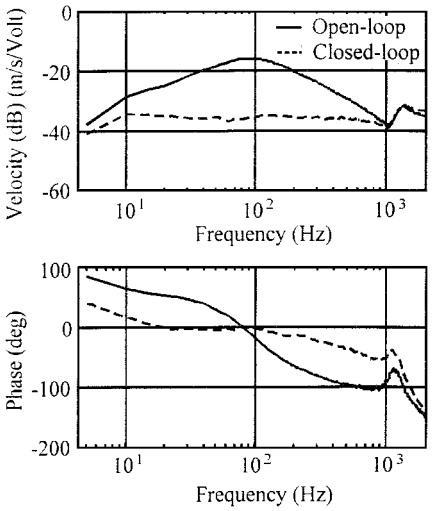

Fig. 8 Measured velocity response of the actuator diaphragm (± 0.26-dB uncertainty).

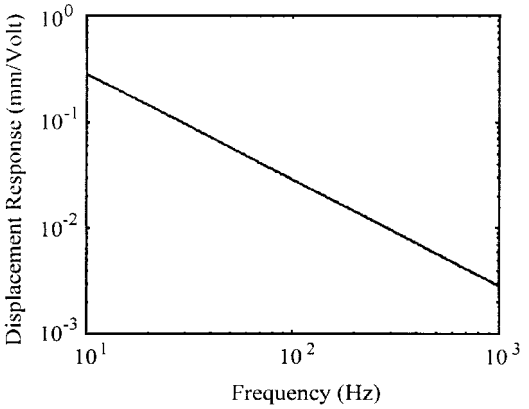

Fig. 9 Computed displacement response of the actuator diaphragm (± 3% uncertainty).

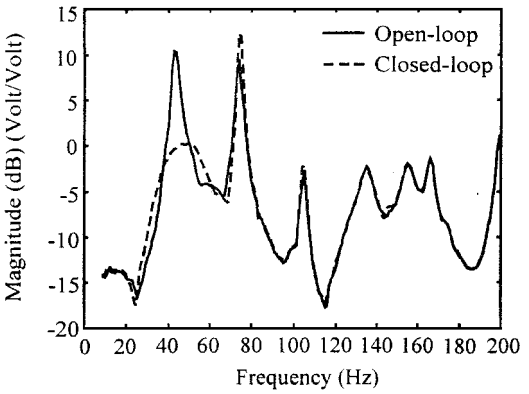

Fig. 10 Average sensor microphone response for the first-mode controller (± 0.51-dB uncertainty).

from 10 to 900 Hz. The phase lag resulting from the actuator dynamics was significantly reduced over this bandwidth. After integration, the assumed constant velocity response of 18 mm/s/V yielded the diaphragm displacement approximation presented in Fig. 9.

Single-Mode Controllers

Initially, experiments were performed to attenuate the response of a single acoustic mode of the fairing. Figures 10 and 11 show the results of a controller designed for the fundamental mode at 47 Hz. Figure 10 presents the averaged open-loop and closed-loop frequency-response functions measured at the sensor microphones relative to the disturbance input. Figure 11 presents the averaged

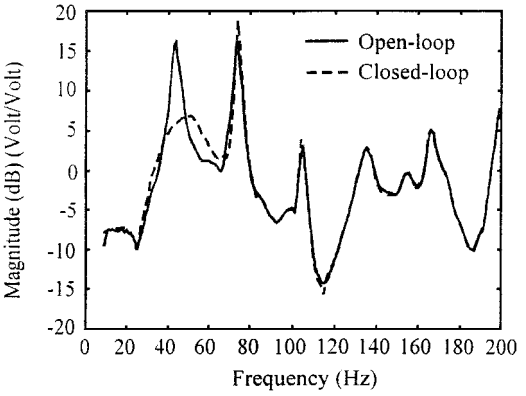

Fig. 11 Average performance microphone response for the first-mode controller (± 0.51-dB uncertainty).

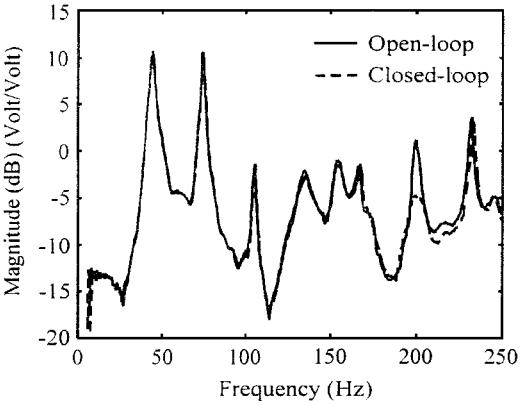

Fig. 12 Average sensor microphone response for the seventh-mode controller (± 0.51-dB uncertainty).

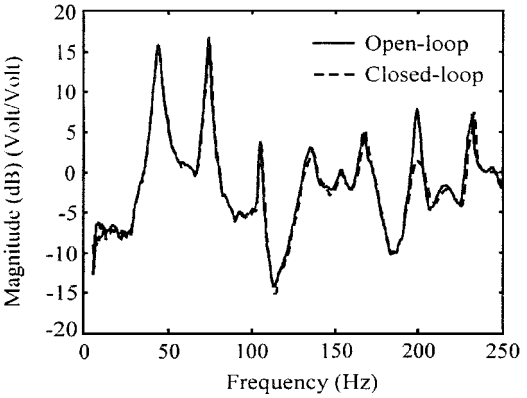

Fig. 13 Average performance microphone response for the seventh-mode controller (± 0.51-dB uncertainty).

open-loop and closed-loop frequency-response functions measured at the performance microphones. Note that Figs. 10 and 11 present the microphone output voltages, which indicate the reduction in the interior SPL achieved by the controller. These results demonstrate that the controller successfully reduced the response of the target mode, both at the sensor microphones and at the performance microphones. This controller was designed to be aggressive, yielding 10 dB of reduction of the target mode at the sensors and performance microphones, respectively, but also creating spillover at the second mode. Computing the open-loop and closed-loop rms pressure reductions indicated that only 0.88 and 0.85 dB of attenuation was achieved at the sensor and performance microphones, respectively, over the 200-Hz bandwidth.

The next experiments investigate the ability of the controller to control higher frequency modes of the fairing. Figures 12 and 13 present the results for a controller designed to target the seventh

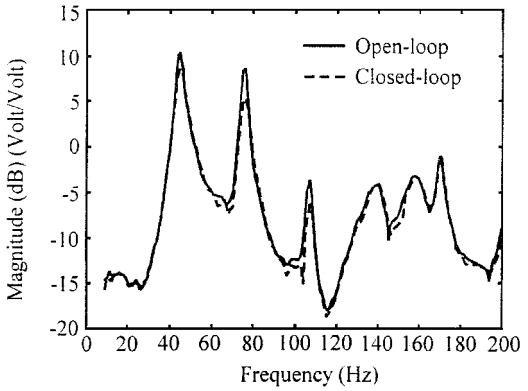

Fig. 14 Average sensor response for the three-mode controller (nonaggressive) (± 0.51-dB uncertainty).

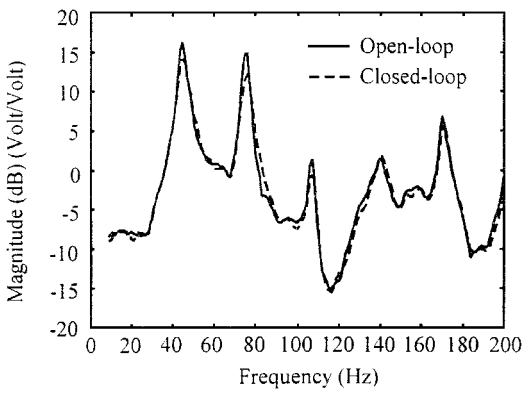

Fig. 15 Average performance microphone response for the three-mode controller (nonaggressive) (± 0.51-dB uncertainty).

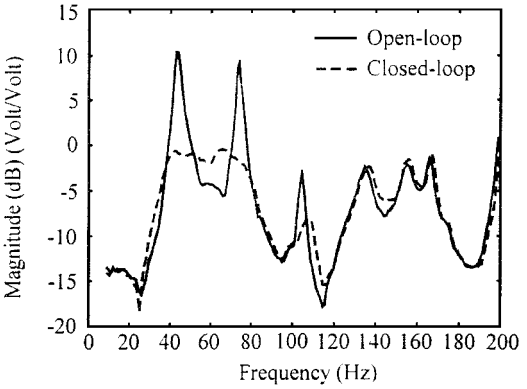

Fig. 16 Average sensor response for the three-mode controller (aggressive) (± 0.51-dB uncertainty).

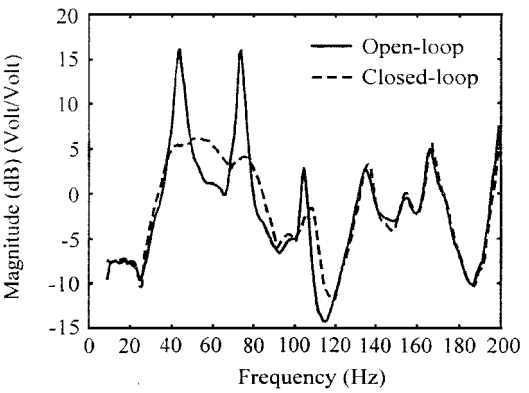

Fig. 17 Average performance microphone response for the three-mode controller (aggressive) (± 0.51-dB uncertainty).

acoustic mode of the fairing at 200 Hz. This controller was less aggressive than the preceding one (i.e., more control effort penalty, see Fig. 2), and yet the response of the target mode was reduced by 6 dB at both the sensor and performance microphone locations. The data indicate that this controller produced very little spillover. In spite of the significant attenuation measured at the single target mode, the overall rms reductions were only 0.17 and 0.32 dB over the 250-Hz bandwidth at the sensor and performance microphones, respectively. However, in both cases, the spatially weighted controller successfully coupled with the target mode and achieved significant attenuation.

Three-Mode Controllers

The next experiments demonstrate the ability of the controller to attenuate multiple acoustic modes. Controllers were designed to attenuate the first, second, and third acoustic modes at 47, 75, and 107 Hz, respectively. The first controller was designed by using a relatively large control effort penalty, which yielded only slight attenuation at each mode, as shown in Figs. 14 and 15. The controller reduced the response of the target modes with negligible spillover. Over the 200-Hz bandwidth, the rms reduction was computed to be 1.19 dB at the sensor microphones and 1.13 dB at the performance microphones.

In the final experiments, a more aggressive controller was implemented, and the results are presented in Figs. 16 and 17. The first and second modes were reduced by approximately 12 dB and the third by 5 dB at the sensor microphones and the performance microphones. The controller had very little effect on the nontarget modes, which is desirable from a stability standpoint. This controller achieved an overall reduction in the rms response at the sensor microphones of 3.46 and 3.30 dB at the performance microphones. This reduction is very significant and is highlighted by measurement of the reduction at arbitrary points throughout the fairing. The first two modes were well controlled, and little more improvement could be achieved at these frequencies. As with the preceding controller, there was very little spillover produced. These results illustrate the importance of achieving an optimal balance of control effort penalty and performance penalty in controller design. These results also demonstrate that the control approach can attenuate multiple modes and achieve significant levels of reduction across the control bandwidth.

Computation of Diaphragm Excursion and Power Requirements

Because the final three-mode controller provided attenuation levels that would be necessary to justify implementing the controller in an actual launch vehicle, the measurements taken from this controller were used to investigate power requirements and actuator diaphragm displacement. The voltage applied to the actuators for various SPLs can be computed by measuring the open-loop pressure responses $p_i(j\omega)$ for the 16 sensor microphones, measuring the controller frequency-response functions $\boldsymbol{H}(j\omega)$ and measuring $\boldsymbol{G}_{\text{mic}}(j\omega)$ and $\boldsymbol{G}_{\text{act}}(j\omega)$. From these measurements, the rms diaphragm displacement and power can be determined as discussed earlier. Results of the displacement and power calculations are presented in Tables 1 and 2, respectively, for the 200-Hz bandwidth.

Table 1 indicates that, for this controller, the diaphragm displacement was less than 2 mm for disturbance levels up to 120 dB. This displacement is within the linear excursion range of the off-the-shelf actuators used in this investigation. At 130 dB, some actuator displacements exceeded the nominal linear excursion limits, and at 140 dB, the predicted excursions were on the order of centimeters. Note that there were considerable discrepancies between the displacements of the various actuators, which indicates that some actuators were not used effectively. Also note that the rms displacement increased roughly an order of magnitude for every 20-dB increase in the SPL (which corresponds to an order of magnitude increase in sound pressure). Because these predictions were based on both microphone measurements, which have an uncertainty of approximately 6.1%, and vibrometer measurements, which have an uncertainty of approximately 3%, the overall uncertainty of these estimates is approximately 9%.

Table 2 shows the power delivered to the speakers that was estimated using Eqs. (18) and (19). Based on the uncertainty of the

Table 1 Predicted rms displacement (millimeters) of speaker diaphragms as a function of SPL (9% uncertainty)

	SPL, dB				
Actuator	100	110	120	130	140
1	0.042	0.132	0.418	1.322	4.181
2	0.056	0.178	0.563	1.779	5.625
3	0.049	0.156	0.494	1.563	4.942
4	0.051	0.160	0.505	1.596	5.047
5	0.049	0.156	0.494	1.562	4.939
6	0.043	0.137	0.432	1.367	4.322
7	0.042	0.132	0.416	1.316	4.162
8	0.045	0.141	0.445	1.407	4.450
9	0.049	0.154	0.488	1.542	4.875
10	0.064	0.201	0.637	2.013	6.366
11	0.064	0.203	0.640	2.025	6.404
12	0.099	0.312	0.987	3.120	9.866
13	0.095	0.300	0.948	2.999	9.483
14	0.076	0.241	0.761	2.407	7.612
15	0.073	0.231	0.730	2.307	7.295
16	0.052	0.163	0.515	1.629	5.150

Table 2 Predicted power (watts) applied to speakers as a function of SPL (27% uncertainty)

	SPL, dB				
Actuator	100	110	120	130	140
1	0.019	0.19	1.9	19	192
2	0.088	0.88	8.8	88	880
3	0.001	0.01	0.1	1	9
4	0.001	0.01	0.1	1	9
5	0.042	0.42	4.2	42	417
6	0.016	0.16	1.6	16	159
7	0.008	0.08	0.8	8	82
8	0.001	0.00	0.0	0	5
9	0.000	0.00	0.0	0	2
10	0.004	0.04	0.4	4	39
11	0.001	0.01	0.1	1	12
12	0.031	0.31	3.1	31	311
13	0.014	0.14	1.4	14	140
14	0.015	0.15	1.5	15	146
15	0.010	0.10	1.0	10	97
16	0.003	0.03	0.3	3	33

microphone measurements, 6.1%, and allowing for uncertainty in frequency response measurements of 0.1%, this yields a total uncertainty in the estimated power requirements of approximately 27%. The values given in Table 2 indicate that the power levels were within the allowable range up to 130 dB. At 140 dB, there were several actuators above the nominal rating. The data indicate that the power requirements increased two orders of magnitude for every 20-dB increase in the SPL. Again, there were considerable variations of the power requirements for each speaker, most notably between speakers 2 and 9.

Conclusions

The preliminary set of experiments presented herein demonstrated that active acoustic control with spatially weighted transducer arrays has the potential to significantly reduce the low-frequency modal response of a launch vehicle fairing. Over 3 dB of reduction was measured throughout the fairing interior over the 20–200-Hz bandwidth. The results demonstrated that the proposed control method successfully coupled with and controlled the target mode(s), attenuating the individual target modes by as much as 12 dB without producing significant spillover.

Feasibility issues for practical implementation of the control system were presented and discussed. For an aggressive three-mode controller, data measured at disturbance levels near 90 dB were extrapolated to predict rms diaphragm displacement and power requirements corresponding to higher SPLs. The data indicated that the required power levels on some speakers exceeded 100 W above 130 dB. However, the diaphragm displacement was less than a few millimeters below 130 dB. The displacement and power requirements are not unrealistic at low frequency, where levels are approximately 130 dB, and may be achieved with better designed actuators and optimization of the number and placement of the actuators.

Acknowledgments

The authors would like to gratefully acknowledge the partial support for this research provided under the Air Force Office of Scientific Research Presidential Early Career Award for Scientists and Engineers, Grant F49620-98-1-0383, monitored by Brian Sanders and Daniel Segalman. We would also like to express our gratitude to the U.S. Air Force Research Laboratory for providing the rocket fairing model used in these experiments.

References

[1]Leo, D. J., and Anderson, E. H., "Vibroacoustic Modeling of a Launch Vehicle Payload Fairing for Active Acoustic Control," AIAA Paper 98-2086, April 1998.

[2]Shen, F., and Pope, D., "Design and Development of Composite Fairing Structures for Space Launch Vehicles," Society of Automotive Engineers, TP 901836, Oct. 1990.

[3]Bradford, L., and Manning, J., "Attenuation of Cassini Spacecraft Acoustic Environment," *Sound and Vibration*, Vol. 30, No. 10, 1996, pp. 30–37.

[4]Weissman, K., McNelis, M. E., and Pordan, W. D., "Implementation of Acoustic Blankets in Energy Analysis Methods with Application to the Atlas Payload Fairing," *Journal of the Institute of Environmental Sciences*, Vol. 37, No. 4, 1994, pp. 32–39.

[5]Niezrecki, C., and Cudney, H. H., "Preliminary Review of Active Control Technology Applied to the Fairing Acoustic Problem," *Proceedings of the AIAA/ASME/AHS Adaptive Structures Forum*, AIAA, Reston, VA, 1996, pp. 101–108; also AIAA Paper 96-1275, 1996.

[6]Lane, S. A., and Clark, R. L., "Dissipative Feedback Control of a Reverberant Enclosure Using a Constant Volume Velocity Source," *Journal of Vibration and Acoustics*, Vol. 120, No. 4, 1998, pp. 987–993.

[7]Lane, S. A., and Clark, R. L., "Improving Loudspeaker Performance for Active Noise Control Applications," *Journal of the Audio Engineering Society*, Vol. 46, No. 6, 1998, pp. 508–519.

[8]Lane, S. A., "Active Noise Control in Acoustic Enclosures Using a Constant Volume Velocity Source," Ph.D. Dissertation, Dept. of Mechanical Engineering and Material Science, Duke Univ., Durham, NC, March 1999.

[9]Shirahatti, U. S., and Crocker, M. J., "Standing Waves," *Encyclopedia of Acoustics*, Vol. 1, edited by M. J. Crocker, Wiley, New York, 1997, pp. 81–89, Chap. 7.

[10]Burke, S., and Hubbard, J., "Spatial Filtering Concepts in Distributed Parameter Control," *Journal of Dynamic Systems, Measurement and Control*, Vol. 112, No. 4, 1990, pp. 565–573.

[11]Burke, S., Hubbard, J., and Meyer, J., "Distributed Transducers and Colocation," *Mechanical Systems and Signal Processing*, Vol. 7, No. 4, 1993, pp. 349–361.

[12]Clark, R. L., Saunders, W. R., and Gibbs, G. P., *Adaptive Structures, Dynamics and Control*, 1st ed., Wiley, New York, 1998, pp. 212–219, 310–312, and 340–354.

[13]Fuller, C., Elliott, S., and Nelson, P., *Active Control of Vibration*, 1st ed., Academic Press, New York, 1996, pp. 141–143.

[14]Morgan, D. R., "An Adaptive Modal-Based Active Control System," *Journal of the Acoustical Society of America*, Vol. 89, No. 1, 1991, pp. 248–256.

[15]Skogestad, S., and Postlethwaite, I., *Multivariable Feedback Control*, 1st ed., Wiley, New York, 1996, pp. 349–369, 452, 453.

[16]Juang, J., *Applied System Identification*, 1st ed., Prentice–Hall, Englewood Cliffs, NJ, 1994, pp. 133–139.

[17]*Simulink, Dynamic Simulation for Matlab*, Ver. 3.0, Release 11, MathWorks, Natick, MA, Sept. 1998.

[18]*Matlab, The Language of Technical Computing*, Ver. 5.3, Release 11, MathWorks, Natick, MA, Jan. 1999.

[19]*μ-Analysis and Synthesis Toolbox*, Ver. 3.0.4, Release 11, MathWorks, Natick, MA, April 1998.

[20]Balabanian, N., and Bickart, T. A., "Power and Energy," *The Electrical Engineering Handbook*, 1st edition, edited by R. C. Dorf, CRC Press, Boca Raton, FL, 1993, Sec. 3.4, pp. 81–87.

M. P. Nemeth
Associate Editor